



Real time revealing relaxation dynamics of ultrafast mode-locked lasers

Tianhao Xian, Wenchao Wang , and Li Zhan *

State Key Laboratory of Advanced Optical Communication Systems and Networks, School of Physics and Astronomy, Shanghai Jiao Tong University, Shanghai 200240, China

 (Received 29 April 2021; revised 29 November 2021; accepted 27 February 2022; published 15 March 2022)

Single-shot measurement of ultrashort time with a dispersive temporal interferometer (DTI) paves the way for exploring intracavity dynamics in ultrafast lasers. Here, we report observations of pulse evolution dynamics after mode-locking buildup in ultrafast lasers. We observe the roundtrip time and phase evolution of the mode-locked pulses after buildup, and we unveil that the pulse experiences three different stages before stabilization, i.e., the soliton breathing stage, the relaxation oscillation stage, and the long-term relaxation stage. We find that the gain depletion effect makes the pulse move forward but does not shift its phase, and it can be distinguished by a DTI from the refractive index change. With this, the dynamics of the three stages is analyzed. Moreover, it is unveiled that the gain relaxation dynamics can intensively affect a laser's stability. These results provide additional perspectives on the intracavity dynamics of mode-locked lasers and of complex nonlinear systems, and they can help to improve the laser stability, which may impact laser design, ultrafast diagnostics, and nonlinear optics.

DOI: [10.1103/PhysRevResearch.4.013202](https://doi.org/10.1103/PhysRevResearch.4.013202)

Mode-locked lasers [1], as important ultrashort pulse sources, are widely used in industrial applications, medical applications, and fundamental research [2,3]. Some of the most precise measurements, from frequency comb metrology [4] to precise timing [5], are performed with mode-locked lasers. Such extreme precision is dependent on the stability of the lasers, which demands a comprehensive understanding of mode-locking dynamics, especially the roundtrip time and carrier phase evolution. In addition to their widespread applications, mode-locked lasers constitute an ideal platform for the fundamental observation of complex nonlinear dynamics, including rogue waves [6], soliton molecules [7,8], soliton explosions [9], and pulsation of soliton bunches [10], making it essential for such fundamental science observation to study mode-locking dynamics.

Mode-locking is a complex phenomenon in which quantities of modes are locked into the same phase to generate ultrashort pulses, even short down to optical cycles [11,12]. The pulse evolution dynamics is determined by the interplays between the pulse and the cavity components, which have been observed extensively since the 1990s [13,14]. Recently, using the dispersive Fourier transform (DFT) technique [7,8,15,16], some mode-locking buildup dynamics have been observed, such as the mode-locking buildup [16–20], the birth and extinction of solitons [21–23], the transition from Q-switching to mode-locking [24], and transient mode-locking

[25]. In these studies, the lasers are considered to be stationary after the buildup process because the single-shot spectrum is stable. However, in the buildup process, the dramatic change in the intracavity photon number changes the gain and loss substantially [26]. Since the lifetime of the gain medium is usually much longer than the roundtrip time [27], the interplay between the gain medium and the pulse pushes the laser off the steady state [28], suggesting that the pulses should experience a relaxation process before stabilization. Although the spectrum is stable, the relaxation may introduce roundtrip time and phase jitters to the pulses, which is directly connected to the laser's stability [29]. However, the observation of such a stabilization process is mitigated by the lack of accurate ultrafast measurements.

Keeping in mind this fundamental physical phenomenon, the salient questions that naturally arise are to guess how the laser relaxes to the steady state and how the relaxation affects the pulses. Resolving such questions can help us to understand the interplay between the soliton and the cavity components, which may lead to the observation of some nonlinear phenomena such as rogue waves [6], the Fermi-Pasta-Ulam paradox [30], breathing solitons [15], and turbulence [31]. Moreover, the mode-locking relaxation is linked to the instability dynamics, such as the Q-switching instability [32] and timing jitter, which is unwanted in high-precision measurements such as a frequency comb [33] and multiphoton microscopy [3]. Therefore, the observation of mode-locking relaxation can help to optimize the laser design in order to suppress or avoid these instabilities, which is attractive in practical applications.

Here, with a single-shot time-measurement technique, namely the dispersive temporal interferometer (DTI) [34,35], we monitor the roundtrip time and phase evolutions of mode-locked pulses during the relaxation process. Based on time and phase evolution, we reveal three distinct stages during the

*Corresponding author: lizhan@sjtu.edu.cn

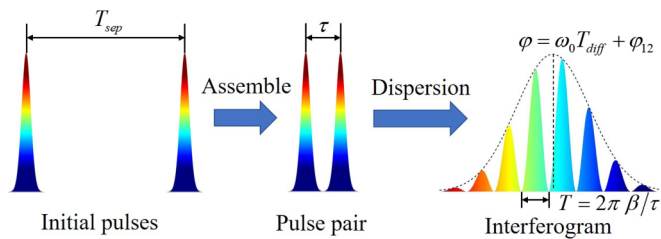


FIG. 1. Capturing the interaction of different pulses with DTI.

relaxation process, i.e., the soliton breath stage, the relaxation oscillation stage, and the long-term relaxation stage. Theoretically, we propose that the gain depletion can accelerate the pulses, and we analyze the different influence of gain depletion and the refractive index change on the pulse. These discoveries can enhance our understanding of the dynamics of mode-locked lasers, and they can help to fabricate highly stable ultrafast lasers for precision measurement applications.

Using DTI, two separated pulses (duration in femtoseconds) with a separation T_{sep} and a phase difference φ_{12} are assembled into a close-spaced pulse pair, as shown in Fig. 1. This requires the former pulse to pass a longer distance than the latter, which introduces a time difference T_{diff} for both pulses. After this, their separation is $\tau = \pm(T_{\text{sep}} - T_{\text{diff}})$ (several picoseconds or subpicoseconds). Then, they are stretched with large dispersion into nanosecond pulse, which is much wider than the initial pulse. The large dispersion can map the frequency ω of the pulse pair into the time domain t , and the relation is $\omega - \omega_0 = t/\beta$, with β the total dispersion and ω_0 the carrier frequency. Note that the reference zero time ($t = 0$) corresponds to the frequency ω_0 . Therefore, the DTI can encode the time separation τ and relative phase φ of the pulse pair into the temporal interferogram, which reads [36,37]

$$I(t) \approx (1/\beta)|E(t/\beta)|^2[1 + \cos(\tau t/\beta + \omega_0 T_{\text{diff}} + \varphi_{12})], \quad (1)$$

where $E(\omega - \omega_0)$ represents the Fourier transform of the envelope of the pulse, and $\omega - \omega_0$ is displaced by t/β because the frequency is mapped into the time domain. One interferogram is displayed in Fig. 1, in which the interferogram phase $\varphi = \omega_0 T_{\text{diff}} + \varphi_{12}$, and the fringe period $T = 2\pi\beta/\tau$. For two different solitons in a multipulse laser, the interferogram evolution maps the soliton interaction. For two pulses from adjacent roundtrips in a single-pulse laser, their separation is the roundtrip time, $T_{\text{sep}} \equiv T_r$. Although the absolute value of T_r is inaccessible as $T_{\text{diff}} \gg \tau$, the evolutions of T_r and φ_{12} are written into τ and φ by

$$\delta T_r = \delta \tau, \quad (2a)$$

$$\delta \varphi = \delta \varphi_{12}, \quad (2b)$$

where $\delta x = x - C$, x represents T_r , τ , φ_{12} , φ , and C is a constant. Therefore, the DTI technique is an effective method to real-time monitor the evolution of the roundtrip time and the phase shift in a mode-locked laser. In the following, we assume the constant for φ is zero, and we use φ to express the phase evolution.

There are three potential evolutions in the time interferogram: (i) only T_r changes, which makes τ and φ change

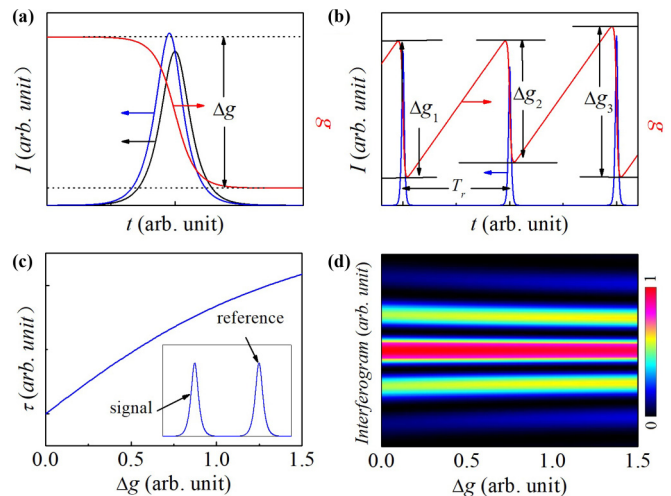


FIG. 2. Time shift due to gain depletion. (a) Scheme of the gain depletion across an amplified soliton. (b) Scheme of the gain depletion at different roundtrips. (c) Time separation of signal pulse and reference pulse as a function of gain depletion. The inset plots the two pulses. (d) Time interferogram evolution at different gain depletion.

synchronously; (ii) only φ changes; and (iii) τ changes but φ is constant. In the following, we will list several effects that can impact the pulse in the laser, and we simulate the interferogram change after commuting with the effect.

First, the Kerr effect can slow down the pulse through increasing the momentary refractive index [38]. The change of the Kerr effect will immediately reform φ [case (ii)]. Since the cavity length is fixed, the roundtrip time is mainly affected by the refractive index and gain depletion [39,40]. The refractive index change will change the effective cavity length, which varies τ and φ synchronously, corresponding to case (i). However, the gain depletion effect can bring the pulse forward [41,42], which is much more complex.

Because the lifetime of the gain medium τ_g is much longer than the pulse duration, the energy transferred to the pulse cannot be replenished immediately, inducing gain depletion during the pulse passing, as shown in Fig. 2(a). Therefore, the gain is time-variant when the pulse passes, and the tail of the pulse sees a smaller gain than does the front [the red line in Fig. 2(a)]. Thus, this effect can reform the pulse envelope and make the pulse move forward [the blue line in Fig. 2(a)], but it does not change the phase velocity.

The time-dependent gain g can be described by the rate equation:

$$\frac{dg}{dt} = \frac{g_0 - g}{\tau_g} - \frac{g|\psi(t)|^2}{E_g}, \quad (3)$$

where g_0 is the small signal gain, E_g is the gain saturation energy, and $\psi(t)$ is the pulse envelope. Since the energy of the pulse $E_s = \int |\psi(t)|^2 dt$ is much smaller than E_g and the pulse duration is much smaller than the roundtrip time, the gain depletion can be measured as $\Delta g = g_i E_s / E_g$, where g_i corresponds to the gain just before the pulse arrives. The value of Δg is determined by E_s and g_i . Figure 2(b) shows the gain depletion under different pulse energy. Then, we consider the

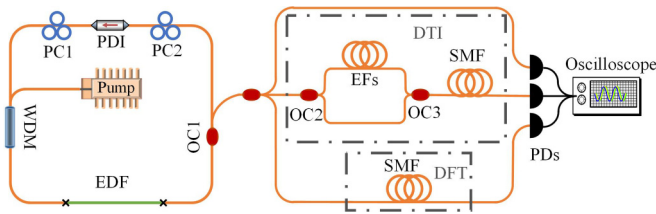


FIG. 3. Experimental setup. The left part is the fiber laser, while the right part is the real-time detection system. WDM: wavelength division multiplexer; OC, optical coupler; EF, extra fibers. The total length of EFs is equal to the cavity length, so the DTI captures the interference of two pulses from adjacent roundtrips. A detailed setup of DTI is shown in Fig. S3.

loss of the laser. Under stable operation, the total gain is equal to the total cavity loss. Considering the gain depletion effect, the net gain of the cavity is time-dependent. We assume that the loss is a constant, and then the net gain can be expressed as [39]

$$g_{\text{net}}(t) = \Delta g \left(1 - \frac{2}{E_g} \int_{-\infty}^t |\psi(t')|^2 dt' \right). \quad (4)$$

Therefore, the pulse envelope $\psi'(t)$ after the gain-dependent effect is $\psi'(t) = \psi(t) \exp[g_{\text{net}}(t)]$.

To illustrate the map of gain depletion on the time interferogram of DTI, we simulate the time interference of two pulses, with the former pulse suffering from the gain depletion effect (the signal pulse) and the latter pulse not (the reference). We assume that the initial solitons have hyperbolic secant envelope $\psi(t) = \text{sech}(10t)$ and their time separation $\tau = 1$. Due to the forward motion of the former pulse, the separation of the two pulses increases with an increase in the gain depletion parameter Δg , as displayed in Fig. 2(c). Their time interferogram [Fig. 2(d)] indicates that the fringe period decreases with separation, but the interferogram phase has not changed. We would like to point out that when we add chirp to the initial soliton, positive or negative, a similar phenomenon arises. This is because the gain-depletion effect can deform the pulse to make the center of the pulse move forward, but it does not introduce a phase shift [39]. In other words, it can change the group location rather than the phase. Thus, the jitter of gain depletion will change τ , but φ will remain constant, which is just case (iii). In comparison, the time shift due to refractive index change will make φ change with τ synchronously [43]. The change of interferogram may come from one of the three cases, or their superposition, and the roundtrip time change and/or the phase shift can be recognized from the interferogram.

The experimental setup is shown in Fig. 3. The laser cavity is 4.82 m long, which consists of 1.36 m erbium-doped fiber (EDF) and 3.46 m standard single mode fiber (SMF). The dispersion is $65 \text{ ps}^2 \text{ km}^{-1}$ for EDF and $-22 \text{ ps}^2 \text{ km}^{-1}$ for SMF at 1550 nm, and the total dispersion is $+0.012 \text{ ps}^2$. The laser is mode-locked by nonlinear polarization rotation through a polarization-dependent isolator (PDI) and two polarization controllers (PCs) [44]. The output laser is split into three portions: the first portion records the instantaneous pulse intensity, the second portion connects a DTI to detect the roundtrip time and phase evolution [43], and the third

portion carries out the spectral measurement [16]. The DTI is fabricated by two 1:1 optical coupler (OCs), dispersion compensation fiber (DCF) and SMF as extra fibers (EFs), and 12 km SMF. The total length of EFs is equal to the cavity length and their total dispersion $|\beta_{\text{EFs}}| < 0.0005 \text{ ps}^2$. Compared with another DTI which contains a delay line in one arm, it can be inferred that the time separation $\tau = T_{\text{diff}} - T_r$. The time-stretching is provided by the dispersion via a 12 km SMF. The signals are detected by a 10 GHz and a 40 GHz photodetector (PD), and captured by a 10 GHz oscilloscope.

The extreme precision of many precise measurements with a mode-locked laser relies on the complexity of the mode-locking dynamics [5,16]. The buildup and the relaxation of the mode-locked state is an ideal platform to study such dynamics because this transition is singular and nonrepetitive and contains various complex dynamics [18,22]. Moreover, the transition among different stages is spontaneous and easily captured. Therefore, we observe the evolution of the roundtrip time and the phase evolution during the buildup and relaxation process of mode-locking. The laser is a typical dispersion-managed mode-locked laser [45] at 1570 nm (optical cycle $T_o = 5.27 \text{ fs}$) with a duration of $\sim 80 \text{ fs}$ and a repetition rate of 42.8 MHz (Fig. S4 in [43]). The mode-locking operation self-starts at 380 mW pump power. Upon the appearance of a pulse signal, it can be triggered and recorded by the oscilloscope.

After the mode-locking buildup, three distinct stages are observed. The first stage, referred to as the soliton breathing stage, is exhibited in Fig. 4: in the first 1000 roundtrips after buildup, the pulse intensity oscillates periodically like breathing [15,34]. The breathing period is ~ 5.5 roundtrips and the breathing depth is higher than 12% at the beginning. Figure 4(a) illustrates the time interferogram evolution during this stage: both the fringe period and the phase change synchronously with the pulse intensity, a peculiar property of breathing soliton [34]. δT_r and φ oscillate with the pulse intensity synchronously, as shown in Fig. 4(b). In 900 roundtrips, breathing attenuates and vanishes gradually. The maximum jitter of φ is 0.45π , much smaller than one cycle. However, the roundtrip time jitter is 73 fs, much larger than the value calculated from phase jitter of 1.1 fs ($\tau = T_o \varphi / 2\pi$). This can be explained via the gain depletion theory: the pulse advancement is proportional to the magnitude of gain depletion, and the latter in each roundtrip is dominated by the pulse intensity [29]. Hence, when the intensity jitters violently, the advancement oscillates synchronously, leading to the roundtrip time change. Since such a change does not tune the pulse phase, δT_r and φ display an evident mismatch. Therefore, the breathing stage highlights that the gain depletion can affect the timing jitter of the mode-locked laser [46].

Figures 4(c) and 4(d) show the pulse dynamics in the soliton breathing stage. The trajectory in Fig. 4(c) shows that the soliton traces first the outer cycle; as the breathing attenuates, the trajectory moves in; when the breathing vanishes, the trajectory reaches a fixed point. This may be because of the gain change: with the mode-locking buildup, the gain decreases sharply [16]. The gain cannot support the stable pulse output, leading to soliton breathing [15]. However, with the attenuation of other fluctuations and the adjustment of the laser, the gain restores gradually, which stabilizes the laser to a fixed point.

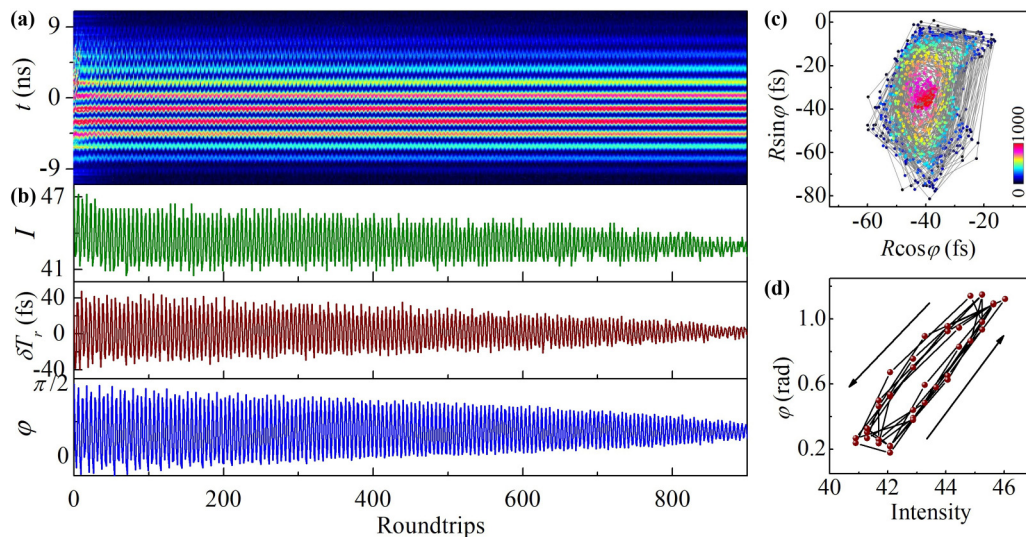


FIG. 4. Soliton breathing stage of mode-locked laser. (a) Time interferogram evolution measured through DTI. (b) Pulse intensity (upper), roundtrip time (middle), and relative phase (lower) evolutions. (c) Relation of δT_r and φ in 1000 roundtrips after mode-locking buildup. The radius (angle) corresponds to δT_r (φ). $R = \delta T_r - C$, with C a constant. (d) φ as a function of intensity for 300–340 roundtrips. Their relation over 900 roundtrips is displayed in Fig. S5 [43].

The linear relation of the relative phase to the pulse intensity [Figs. 4(d) and S2] suggests their direct link to the Kerr effect: the momentary refractive index of the fiber depends on the peak power of the pulse. However, the pulse periodically traces a closed orbit, in which the falling edge is higher than the riding edge while both are linear. This is because the pulse has a different duration at both edges: the pulse is amplified in the rising edge and compressed due to the enhancement of self-phase modulation. In the falling edge, the pulse is attenuated. Due to the drop-off of the self-phase modulation, the pulse is stretched by dispersion.

As illustrated in Fig. 5, the relaxation oscillation stage lasts ~ 7 ms. Figure 5(a) displays the evolution of the interferogram, which shows that the phase oscillates in a period of $\sim 320 \mu\text{s}$. The pulse intensity in Fig. 5(b) exhibits analogous oscillation. Shown in Fig. 5(b), the oscillations of the phase and intensity phase are synchronous, indicating their internal link. The relation of δT_r and φ is shown in Fig. 5(c). The maximum jitter of φ is 0.45 rad, corresponding to 0.38 fs, much smaller than the resolution of δT_r (~ 5 fs). Therefore, the roundtrip time may change with the phase, but it cannot be recognized.

In addition to the oscillation, the phase performs a linear-increase tendency, which is the long-term relaxation stage that will be discussed later. Subtracting such a linear increase by $\varphi' = \varphi - aT$ (a is a coefficient), the relation of the phase to the intensity is shown in Fig. 5(d). φ increases with intensity linearly, indicating that the phase jitter originates from intensity jitter, which is attributed to the Kerr effect. The error in Fig. 5(d) comes mainly from the measurement error of the intensity. Different from the soliton breathing stage, there is no obvious difference in the rising and falling edges, which highlights that the pulse envelope has no change in this stage. This oscillation may come from the relaxation oscillation of the gain medium [47]: the dramatic change of the intracavity photon number as the pulse builds up breaks the balance of photon number and gain; because the lifetime of the gain

level in EDF (~ 10 ms) [48] is much longer than the roundtrip time, the gain oscillates with the pulse intensity in a long time before reaching the equilibrium state.

After the oscillation, the laser experiences a long-term relaxation stage in several seconds, as shown in Fig. 6. During

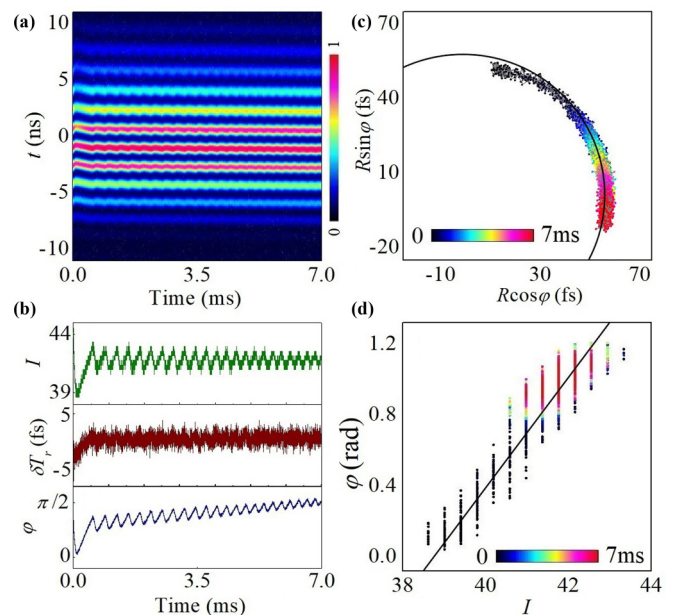


FIG. 5. Relaxation oscillation in 7 ms after mode-locking buildup. (a) Single-shot time interferogram evolution, which is captured using the ultrasegmentation method with $1 \mu\text{s}$ holdoff time. Therefore, the adjacent interferograms have an interval of $1 \mu\text{s}$. A total of 7000 interferograms are presented in (a), which lasts 7 ms. (b) Pulse intensity, time separation, and relative phase. (c) Relation of δT_r and φ . The scatters are the experimental data, and the black line is a theoretical line of Eq. (3). (d) φ as a function of intensity. The black line is the fitting of the scatters.

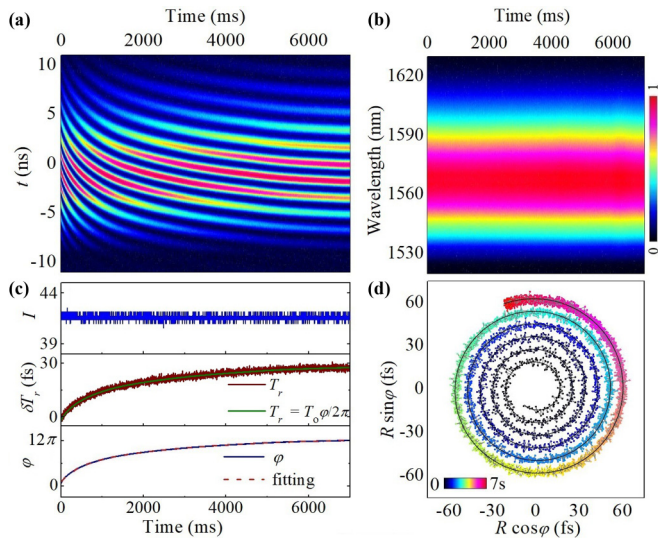


FIG. 6. Relaxation in 7 s after mode-locking buildup. (a) Time interferogram evolution over 7 s. The time interval of adjacent interferograms is 1 ms. (b) Spectrum evolution. (c) Pulse intensity, time separation, and relative phase evolutions. The olive line in the middle is calculated by the blue line (φ) in the lower part through Eq. (2). The red dashed line in the lower part is the exponential fitting. (d) Relation of δT_r and φ . The black line is the fitting of scatters with Eq. (2).

this stage, the pulse intensity and the spectrum are stationary, but the interferogram illustrates an exponential evolution in the time domain [Figs. 6(a)–6(c)], which is beyond the ability of the DFT technique. The middle of Fig. 6(c) displays that the roundtrip time increases by 30 fs. Meanwhile, φ increases synchronously with T_r [Fig. 6(c)]. Also, we calculate δT_r using $\delta T_r = T_0 \varphi / 2\pi + C$ [the olive line in the middle of Fig. 6(c)], which fits well with δT_r . Figure 6(d) shows the relation of δT_r and φ : the pulse traces a trajectory ($R = T_0 \varphi / 2\pi + C$) from the outer cycle to the inner one, and it finally reaches a fixed point with a constant roundtrip time and phase. Unambiguously, the roundtrip time change is attributed to the refractive index change. In view of the constant pulse intensity, it can be inferred that the refractive index change may originate from the relaxation of the gain medium or the thermal effect. According to the Kramers-Kronig (KK) relation [49], the change of population inversion in EDF modifies its refractive index. In addition, the thermal effect induced by the mode-locking can also change the temperature of the fiber and influence the refractive index. The exponential fitting in Fig. 6(c) highlights

the relaxation process in this laser. Then, the roundtrip time evolution during this stage is

$$T_r = T_{r0} - T_{rc} \exp(-t/\tau_r), \quad (5)$$

where T_{r0} is the roundtrip time after relaxation, T_{rc} is the relaxation coefficient, and τ_r is the relaxation time. In our experiment, T_{rc} is 30 fs, and $\tau_r \approx 400$ ms. The relaxation time is longer than the lifetime of the upper level in EDF [48], which is caused by the feedback mechanism of the laser. In a longer timescale, timing jitter is observed although the intensity is stable (Fig. S7), indicating that the laser suffers from timing jitter [50].

In some precise measurements with mode-locked lasers, the precision relies on the mode-locking dynamics. The roundtrip time and pulse phase should be accurately controlled to maintain the stability for the most precise measurements. The three stages after mode-locking buildup mirror that the gain relaxation dynamics [51] can intensively affect the laser's time and/or phase stability, and the relaxation takes longer than the gain medium's lifetime. Moreover, in some other types of mode-locked lasers, such as Kerr lens mode-locked lasers, such relaxation can also be observed. But it takes much less time for the pulse to pass the gain crystal there than pass the EDF, so the relaxation effect may be much weaker. These observations may impact the laser design and help to improve the laser performance.

In conclusion, we have demonstrated the application of DTI for tracing the pulse evolution in mode-locked lasers. With this method, we have resolved the evolutions of a pulse's roundtrip time and the relative phase after the buildup of mode-locking, and we have unveiled the stages of soliton breath, relaxation oscillation, and long-term relaxation. We have analyzed the influence of gain depletion and the refractive index change on the roundtrip time and phase of a pulse in a fiber laser, and we have mapped the model of soliton evolution dynamics in three stages. Moreover, the single-shot measurement of roundtrip time and relative pulse phase is extremely valuable for pulse synthesis, frequency comb, and precise timing, and we expect that our method can find further applications in these areas.

This work was funded by the National Natural Science Foundation of China (NSFC) (Grant No. 11874040), the China Postdoctoral Science Foundation (Grant No. 2021M702149), Shanghai Sailing Program (Grant No. 22YF1420000), and the Foundation for leading talents of Minhang, Shanghai.

[1] U. Keller, Recent developments in compact ultrafast lasers, *Nature (London)* **424**, 831 (2003).
 [2] M. E. Fermann and I. Hartl, Ultrafast fibre lasers, *Nat. Photon.* **7**, 868 (2013).
 [3] C. Xu and F. W. Wise, Recent advances in fiber lasers for nonlinear microscopy, *Nat. Photon.* **7**, 875 (2013).
 [4] T. Udem, J. Reichert, R. Holzwarth, and T. W. Hänsch, Absolute Optical Frequency Measurement of the Cesium D1 Line with a Mode-Locked Laser, *Phys. Rev. Lett.* **82**, 3568 (1999).

[5] M. Xin, K. Şafak, and F. X. Kärtner, Ultra-precise timing and synchronization for large-scale scientific instruments, *Optica* **5**, 1564 (2018).
 [6] D. R. Solli, C. Ropers, P. Koonath, and B. Jalali, Optical rogue waves, *Nature (London)* **450**, 1054 (2007).
 [7] G. Herink, F. Kurtz, B. Jalali, D. R. Solli, and C. Ropers, Real-time spectral interferometry probes the internal dynamics of femtosecond soliton molecules, *Science* **356**, 50 (2017).

- [8] K. Krupa, K. Nithyanandan, U. Andral, P. Tchofo-Dinda, and P. Grelu, Real-Time Observation of Internal Motion within Ultrafast Dissipative Optical Soliton Molecules, *Phys. Rev. Lett.* **118**, 243901 (2017).
- [9] A. F. J. Runge, N. G. R. Broderick, and M. Erkintalo, Observation of soliton explosions in a passively mode-locked fiber laser, *Optica* **2**, 36 (2015).
- [10] Z. Wang, Z. Wang, Y. Liu, R. He, J. Zhao, G. Wang, and G. Yang, Self-organized compound pattern and pulsation of dissipative solitons in a passively mode-locked fiber laser, *Opt. Lett.* **43**, 478 (2018).
- [11] H. Luo, L. Zhan, L. Zhang, Z. Wang, C. Gao, and X. Fang, Generation of 22.7-fs 2.8-nJ pulses from an erbium-doped all-fiber laser via single-stage soliton compression, *J. Lightwave Technol.* **35**, 3780 (2017).
- [12] U. Morgner *et al.*, Sub-two-cycle pulses from a Kerr-lens mode-locked Ti:sapphire laser, *Opt. Lett.* **24**, 411 (1999).
- [13] N.-W. Pu, J.-M. Shieh, Y. Lai, and C.-L. Pan, Starting dynamics of a cw passively mode-locked picosecond Ti:sapphire/DDI laser, *Opt. Lett.* **20**, 163 (1995).
- [14] H. Li, D. G. Ouzounov, and F. W. Wise, Starting dynamics of dissipative-soliton fiber laser, *Opt. Lett.* **35**, 2403 (2010).
- [15] J. Peng, S. Boscolo, Z. Zhao, and H. Zeng, Breathing dissipative solitons in mode-locked fiber lasers, *Sci. Adv.* **5**, eaax1110 (2019).
- [16] G. Herink, B. Jalali, C. Ropers, and D. R. Solli, Resolving the build-up of femtosecond mode-locking with single-shot spectroscopy at 90 MHz frame rate, *Nat. Photon.* **10**, 321 (2016).
- [17] X. Liu, X. Yao, and Y. Cui, Real-Time Observation of the Buildup of Soliton Molecules, *Phys. Rev. Lett.* **121**, 023905 (2018).
- [18] J. Peng, M. Sorokina, S. Sugavanam, N. Tarasov, D. V. Churkin, S. K. Turitsyn, and H. Zeng, Real-time observation of dissipative soliton formation in nonlinear polarization rotation mode-locked fibre lasers, *Commun. Phys.* **1**, 20 (2018).
- [19] X. Liu and Y. Cui, Revealing the behavior of soliton buildup in a mode-locked laser, *Adv. Photon.* **1**, 016003 (2019).
- [20] H. J. Chen, M. Liu, J. Yao, S. Hu, J. B. He, A. P. Luo, W. C. Xu, and Z. C. Luo, Buildup dynamics of dissipative soliton in an ultrafast fiber laser with net-normal dispersion, *Opt. Express* **26**, 2972 (2018).
- [21] Y. Cui and X. Liu, Revelation of the birth and extinction dynamics of solitons in SWNT-mode-locked fiber lasers, *Photon. Res.* **7**, 423 (2019).
- [22] X. Liu and M. Pang, Revealing the buildup dynamics of harmonic mode-locking states in ultrafast lasers, *Laser Photon. Rev.* **13**, 1800333 (2019).
- [23] Y. Zhou, Y.-X. Ren, J. Shi, H. Mao, and K. K. Y. Wong, Buildup and dissociation dynamics of dissipative optical soliton molecules, *Optica* **7**, 965 (2020).
- [24] X. Liu, D. Popa, and N. Akhmediev, Revealing the Transition Dynamics From Q Switching to Mode Locking in a Soliton Laser, *Phys. Rev. Lett.* **123**, 093901 (2019).
- [25] P. Ryczkowski, M. Närhi, C. Billet, J. M. Merolla, G. Genty, and J. M. Dudley, Real-time full-field characterization of transient dissipative soliton dynamics in a mode-locked laser, *Nat. Photon.* **12**, 221 (2018).
- [26] C. R. Menyuk, J. K. Wahlstrand, J. Willits, R. P. Smith, T. R. Schibli, and S. T. Cundiff, Pulse dynamics in mode-locked lasers: Relaxation oscillations and frequency pulling, *Opt. Express* **15**, 6677 (2007).
- [27] A. M. Weiner, *Ultrafast Optics* (Wiley, New Jersey, 2009).
- [28] O. Svelto, *Principles of Lasers* (Springer, New York, 2010).
- [29] R. Weill, A. Bekker, V. Smulakovsky, B. Fischer, and O. Gat, Noise-mediated Casimir-like pulse interaction mechanism in lasers, *Optica* **3**, 189 (2016).
- [30] Z. Zhang, Y. Zhang, J. Sheng, L. Yang, M. A. Miri, D. N. Christodoulides, B. He, Y. Zhang, and M. Xiao, Observation of Parity-Time Symmetry in Optically Induced Atomic Lattices, *Phys. Rev. Lett.* **117**, 123601 (2016).
- [31] J. M. Soto-Crespo, N. Devine, and N. Akhmediev, Integrable Turbulence and Rogue Waves: Breathers or Solitons? *Phys. Rev. Lett.* **116**, 103901 (2016).
- [32] N. B. Abraham, P. Mandel, and L. M. Narducci, *Progress in Optics* (North-Holland, Amsterdam, 1988).
- [33] T. R. Schibli, I. Hartl, D. C. Yost, M. J. Martin, A. Marcinkevičius, M. E. Fermann, and J. Ye, Optical frequency comb with submillihertz linewidth and more than 10 W average power, *Nat. Photon.* **2**, 355 (2008).
- [34] T. Xian, L. Zhan, W. Wang, and W. Zhang, Subharmonic Entrainment Breather Solitons in Ultrafast Lasers, *Phys. Rev. Lett.* **125**, 163901 (2020).
- [35] T. Xian, W. Wang, and L. Zhan, Dispersive temporal interferometry toward single-shot probing ultrashort time signal with attosecond resolution, *Adv. Photon. Res.* **3**, 2100303 (2022).
- [36] G. P. Agrawal, *Nonlinear Fiber Optics* (Academic, New York, 2013).
- [37] M. T. Kauffman, W. C. Banyai, A. A. Godil, and D. M. Bloom, Time-to-frequency converter for measuring picosecond optical pulses, *Appl. Phys. Lett.* **64**, 270 (1994).
- [38] R. W. Boyd, *Nonlinear Optics* (Elsevier, Singapore, 2009).
- [39] J. N. Kutz, B. C. Collings, K. Bergman, and W. H. Knox, Stabilized pulse spacing in soliton lasers due to gain depletion and recovery, *J. Quantum Electron.* **34**, 1749 (1998).
- [40] K. Sulimany, O. Lib, G. Masri, A. Klein, M. Fridman, P. Grelu, O. Gat, and H. Steinberg, Bidirectional Soliton Rain Dynamics Induced by Casimir-Like Interactions in a Graphene Mode-Locked Fiber Laser, *Phys. Rev. Lett.* **121**, 133902 (2018).
- [41] H. A. Haus, Theory of mode locking with a slow saturable absorber, *IEEE J. Quantum Electron.* **11**, 736 (1975).
- [42] R. V. Gumenyuk, D. A. Korobko, and I. O. Zolotovskii, Stabilization of passive harmonic mode locking in a fiber ring laser, *Opt. Lett.* **45**, 184 (2020).
- [43] See Supplemental Material at <http://link.aps.org/supplemental/10.1103/PhysRevResearch.4.013202> for the detailed description of the concepts and experimental results.
- [44] A. Komarov, H. Leblond, and F. Sanchez, Theoretical analysis of the operating regime of a passively-mode-locked fiber laser through nonlinear polarization rotation, *Phys. Rev. A* **72**, 063811 (2005).
- [45] D. Deng, L. Zhan, Z. Gu, Y. Gu, and Y. Xia, 55-fs pulse generation without wave-breaking from an all-fiber erbium-doped ring laser, *Opt. Express* **17**, 4284 (2009).
- [46] J. Kim, J. A. Cox, J. Chen, and F. X. Kärtner, Drift-free femtosecond timing synchronization of remote

- optical and microwave sources, *Nat. Photon.* **2**, 733 (2008).
- [47] I. Mozjerin, S. Ruschin, and A. A. Hardy, Analysis of relaxation oscillations and gain switching of unidirectional erbium-doped waveguide ring lasers, *IEEE J. Quantum Electron.* **46**, 158 (2010).
- [48] A. Zareanborji, H. Yang, G. E. Town, Y. Luo, and G.-D. Peng, Simple and accurate fluorescence lifetime measurement scheme using traditional time-domain spectroscopy and modern digital signal processing, *J. Lightwave Technol.* **34**, 5033 (2016).
- [49] M. Janos and S. C. Guy, Signal-induced refractive index changes in erbium-doped fiber amplifiers, *J. Lightwave Technol.* **16**, 542 (1998).
- [50] Y. Wang, H. Tian, Y. Ma, Y. Song, and Z. Zhang, Timing jitter of high-repetition-rate mode-locked fiber lasers, *Opt. Lett.* **43**, 4382 (2018).
- [51] F. Krausz, M. E. Fermann, T. Brabec, P. F. Curley, M. Hofer, M. H. Ober, C. Spielmann, E. Wintner, and A. J. Schmidt, Femtosecond solid-state lasers, *J. Quantum Electron.* **28**, 2097 (1992).